Synthesis and Characterization of Soluble and Thermally Stable Polypyrrole-DBSA Salts

[1]Salma Bilal, [1]Mohammad Sohail and [2]Anwar-ul-Haq Ali Shah*
[1]*National Center of Excellence in Physical Chemistry University of Peshawar, 25120 Peshawar, Pakistan.*
[2]*Institute of Chemical Sciences, University of Peshawar, 25120 Peshawar, Pakistan.*
anwhq_pk@yahoo.com*

(Received on 13th May 2013, accepted in revised form 7th March 2014)

Summary: In the present study, an attempt has been made to synthesize soluble PPy via inverse emulsion polymerization pathway using benzoyl peroxide as an oxidant and dodecylbenzenesulfonic acid (DBSA) as dopant as well as a surfactant. A mixture of chloroform and 2-butanol was used as dispersion medium for the first time. Pyrrole polymerized into PPy inside the micelle under these conditions. The influence of synthesis parameters such as amount of pyrrole, benzoyl peroxide (BPO) and DBSA on the percent yield and other properties of the resulting PPy was studied. The synthesized PPy was found to be completely soluble in DMSO, DMF, THF, chloroform and *m*-cresol *etc*. The structure of PPy and incorporation of DBSA in the polymer backbone was confirmed by FT-IR. UV-Vis spectra of PPy showed correspondence with the electrical conductivity of the prepared salts. SEM micrographs showed the typical granular morphology of PPy-DBSA. TGA and XRD of the prepared PPy samples were also studied and explained.

Keywords*:* Conducting polymers; Soluble polypyrrole; FT-IR; TGA; SEM; XRD.

Introduction

Inherently conducting polymers (ICPs) with large π-conjugated system have attracted considerable interest due to their prospective wide applications in light emitting diodes (LEDs) , chemical and biological sensors, photovoltaic cells, rechargeable batteries, electrochromic devices, corrosion inhibition, microactuators, antielectrostatic coatings and functional membranes [1] *etc*. Polypyrrole (PPy) is one of the most familiar conducting polymers due to its facile synthesis, good electrical conductivity, biocompatibility and environmental stability [2]. PPy can be synthesized easily either by chemical or electrochemical polymerization. A number of papers discuss the synthesis and properties of PPy films via electrochemical polymerization. However, very little is known about the chemical synthesis of PPy in homogenous solution. Chemical polymerization proceeds readily in the presence of various oxidants, like $K_2S_2O_8$, $FeCl_3$, $(NH_4)_2S_2O_8$ and $CuCl_2$. There are considerable reports on the polymerization of pyrrole in different textile composites [3] and on printed circuit boards [4]. The strong interchain interactions in PPy films make the polymer insoluble in common solvents rendering it highly improcessable, thereby decreasing its scope of applications. Many techniques have been used to deal with these intractable problems. It has been reported that polymerization of substituted pyrrole with long-chain alkyl and sulphonic groups leads to formation of polypyrrole derivatives soluble in some common organic solvents [5]. However, a significant decrease in the electrical conductivity of the polymer is observed in this case, which is due to the decrease of π-conjugation along the polymer chain caused by an increase in torsion angle between the pyrrole rings. Moreover, this type of polymerization is tedious and leads to low efficiency and high cost.

Investigations have shown that PPy synthesized in colloidal dispersion in the presence of external stabilizer shows good solubility and exhibits unique physicochemical characteristics that can widely be used in sensors, biomedicines, supercapacitors and carbon nanomaterial precursors [6]. Colloidal dispersions can be prepared by emulsion, microemulsion and inverse emulsion techniques. Emulsion polymerization is applied where water soluble PPy is required [7]. Microemulsion polymerization is used to prepare nanostructures of PPy. This method permits particles to transfer into the spherical aggregates by surfactant templates [8]. Inverse emulsion polymerization is a recent technique used for the synthesis of high molecular weight and highly soluble polymer. This method improves the physical properties of polymer such as solubility in common organic solvents, stability and processibility [9]. The use of surfactants like dodecylbenzenesulfonic acid (DBSA) in emulsion polymerization has greatly increased the solubility of polymers in polar/non- polar solvents [10]. The use of surfactants in polymerization bath is believed to create a reactor vessel in the dispersion medium via micelle formation, in which the monomer is confined in a limited environment and to improve the polymer's physical properties like solubili-

*To whom all correspondence should be addressed.

ty in organic solvents, conductivity, stability and processibility [11]. We have recently reported the synthesis of completely soluble and highly thermally stable polyaniline via a new inverse emulsion pathway [12]. Inverse microemulsion route has been adopted for a number of PPy nanocomposites like PPy-Pd nanospheres [13], graphite/AgCl/PPy nanosheets [14] and Carbon Nanotube/ PPy Core–Shell [15]. There is no exclusive report available on the synthesis and characterization of PPy using inverse emulsion polymerization. In the present paper synthesis of PPy via inverse emulsion polymerization and further characterization of the synthesized materials are reported. The solubility of the synthesized polymer was investigated in various common organic solvents. The synthesized polymer was found to be completely soluble in a so far large number of common organic solvents. The effect of various reaction parameters on the percent yield, intrinsic viscosity, morphology, structure, and crystallinity of PPy has also been investigated. TGA data showed high thermal stability of the polymer up to ~ 450°C.

Results and Discussion

Percent Yield

High percent yield of the product reflects the optimization of various parameters and the potential of the procedure applied. The present technique was found to be effective in this regard. The effect of amount of monomer and the oxidant (BPO) on the % yield of PPy was studied as given in Table-1 and shown in Fig. 1. It was found that high pyrrole concentration leads to a high yield of the polymer. It indicates that large numbers of monomer radicals get the chance of polymerization inside the micelle and thus enough quantity of the polymer is produced [**Error! Bookmark not defined.**].

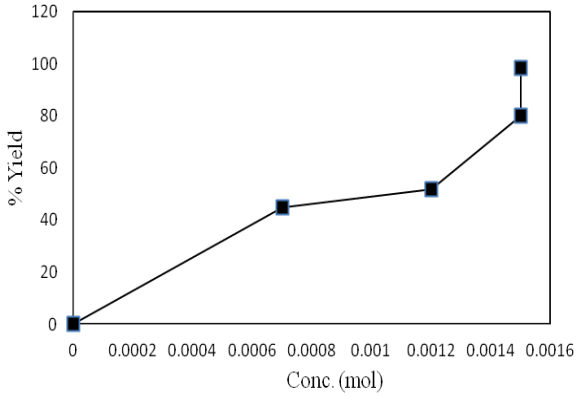

Fig. 1: Effect of amount of monomer on the percent yield of PPy with ≥ 0.02% error.

Table-1: Percent Yield of PPy.

S. No	Sample ID	Pyrrole Conc	BPO Conc	PPy % Yield
1	PPy 1	1.2×10^{-3} mol	0.012 mol	52
2	PPy 2	1.5×10^{-3} mol	0.012 mol	80
3	PPy 3	1.5×10^{-3} mol	0.0012 mol	98.5

Solubility

The presence of long chain conjugated structure make conducting polymers insoluble in aqueous/non-aqueous solvents. One of the main objectives of this study was to synthesize soluble PPy that can easily be processed in its various applications. The solubility of PPy was checked in different common organic solvents. PPy solutions were prepared in selected solvents like DMSO, DMF, THF, *m*-cresol, chloroform and mixtures of other organic solvents. Homogenous solutions were obtained at ambient temperature that determine the complete solubility of PPy in these solvents studied so for, as given in Table-2. Chemical structure of PPy determines its solubility in various solvents. Also, PPy morphology at molecular level has a strong influence on the kinematics of its dissolution. Higher diffusion rates and swelling power of the solvent molecules accelerate the solubility of PPy. A two-step process for the dissolution of PPy has also been proposed. First, swelling of the polymer below θ temperature corresponds to the gradual dispersion of the PPy side chains and then the complete dissolution above θ temperature corresponds to the gradual dispersion of the main chains at molecular level. These dispersions reflect the fact that the cohesion interactions among side chains or main chains of PPy are weakened by the solvent molecules. The effect of relatively polar solvents like DMSO, THF, DMF and *m*-cresol on the solubility is reasonably greater because of dipole-dipole interactions [**Error! Bookmark not defined.**]. Fig. 2 shows that the solubility of PPy is also influenced by the amount of DBSA. As the DBSA amount increases, the solubility of PPy also increases, which is attributed to the fact that high concentration of the dopant in the dispersion medium hinders the cross-linking among PPy chains [**Error! Bookmark not defined.**]. It has been found that these polar solvents build up strong hydrogen bonds with PPy and as a consequence, the polymer dissolves completely in these solvents. The polar oxygen of SO_3^- group in DBSA also increases the solubility of PPy in polar solvents [16].

Table-2: Solubility of PPy in common organic solvents.

S. No	Organic solvent	Minimum solubility (wt./vol %)
	DMSO	~9
	DMF	~9
	THF	~9
	m-cresol	~8
	Chloroform	~7

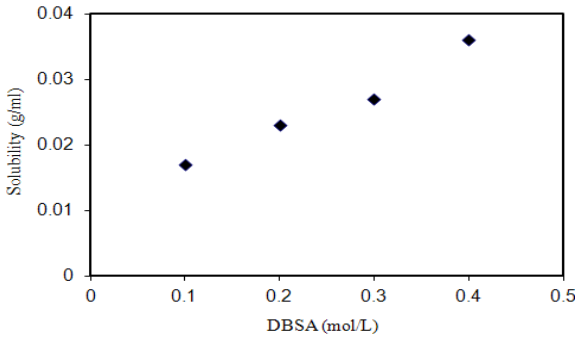

Fig. 2: Effect of amount of DBSA on the solubility of PPy in DMSO (0.071 % error).

Solubility of PPy in these solvents is also governed by the free energy of mixing.

$$\Delta G_m = \Delta H_m - T\Delta S_m \quad (1)$$

where ΔG_m is the free energy change on mixing, ΔH_m is enthalpy change on mixing, T is the absolute temperature and ΔS_m is the entropy change on mixing. A negative value of ΔG_m means that the mixing process occurs spontaneously.

FTIR Analysis

The FT-IR spectra of PPy 1 (a), PPy 2 (b) and PPy 3 (c) is given in Fig. 3 and respective assignments are presented in Table-3. It shows the typical characteristic peaks of PPy which are consistent with that reported in literature [17-19] which means that the prepared salt is that of PPy-DBSA. The peaks in PPy 3 are at a little higher frequency than those of PPy 1 and PPy 2. It is due to the degree of oxidation and length of conjugated chain that influence the doping level of the PPy which in turn affects the ratio of transmittance maxima [20]. The characteristic vibration peaks of PPy-DBSA are in the range of 700-1800 cm^{-1}. The peaks at 1544-1550 cm^{-1} and 1460 cm^{-1} are attributed to C=C/C–C and C–N stretching vibrations in pyrrole rings respectively. The broad peaks at around 1160-1180 cm^{-1} are associated with the breathing vibration of the pyrrole ring in the PPy chain. The peaks at 1304-1320 cm^{-1} correspond to N-H bending. The bands at 1030-1040 cm^{-1} are assigned to the in-plane deformation vibration of C-H and N-H while the out-of-plane deformation vibration band for C-H is located at about 906 cm^{-1}. The peaks at 920-960 cm^{-1} in all the three samples (PPy 1, PPy 2 and PPy 3) correspond to bipolaron bands. The broad peak at 1182 cm^{-1} is related to the S=O stretching vibration of SO_3^- of the DBS^{-1} in PPy. It has been found that the skeletal vibrations of PPy, that involve the π-electrons delocalization, are influenced by the doping of PPy. The typical peaks at 2352-2364 cm^{-1} are considered to be due to aromatic and aliphatic C-H stretching vibration. It means that the IR peaks above 2000 cm^{-1} are dominated by the DBS units, while the IR absorption below 2000 cm^{-1} is affected by the pyrrole units in the PPy-DBSA. Thus the FT-IR analysis confirms the formation of PPy and the presence of pyrrole and DBSA in this synthesized material. The assignments given in Table-3 are in agreement with that given in literature [**Error! Bookmark not defined.**-].

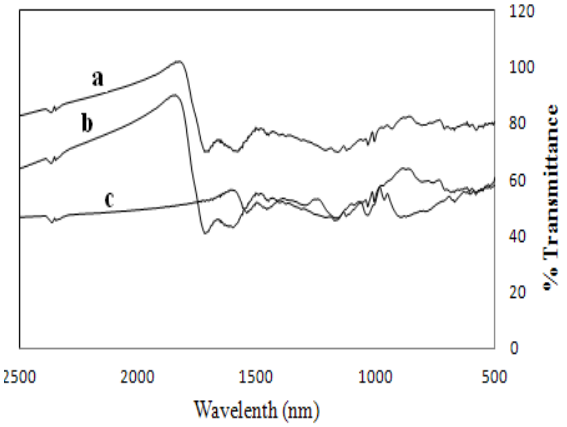

Fig. 3: FTIR spectra of PPy 1 (a), PPy 2 (b) and PPy 3 (c).

Table-3: Assignment of the bands in IR spectra of different PPy samples.

S. No	IR Frequency of absorption (cm^{-1})			Assignment
	PPy 1	PPy 2	PPy 3	
1	2358-2370	2355-2368	2352-2370	υ C-H
2	1720	1720	1757	ω Carbonyl group
3	1587	1573	1544	υ C=C/C-C
4	1460	1452	1460	υ C-N
5	1320	1340	1304	s N-H
6	1200	1215	1182	υ S=O
7	1166	1176	1175	υ C=N
8	1160	1165	1160	b Pyrrole ring
9	1038	1040	1040	β C-H
10	1033	1033	1035	β N-H
11	974	974	966	Bipolaron bands
12	930	935	906	ω C-H
13	715	730	720	ω N-H
14	580	580	582	υ C-S/S-O

υ- Stretching vibration, ω- Out-of-plane wagging, b- Breathing, s- Bending, β- In-plane wagging

Morphology

SEM was performed to analyze the morphology of PPy in various amounts of the monomer. The results are shown in Fig. 4. SEM analysis at higher magnification reveals the homogeneous distribution of DBSA in PPy chains. It is seen that the clusters and granular structure of PPy is sustained in all the three samples with varying concentration of the monomer [24]. Fig. 4 (a) shows smooth and beading surface morphology of PPy with obvious crakes. The uniform structure assists the arrangement of electrical conductive network within the PPy chain [25].

Fig. 4 (b) and (c) show that PPy has globular structure due to the formation of aggregates, which results in a uniform surface morphology known as "cauliflower" [26]. It is also called "broken eggshell" like morphology due to phase segregation. The porous nature of all these samples can be applied in adsorption and gas sensing technologies while the pellet (Fig 4 (a)) like behavior is best fit for the use in biosensors [27].

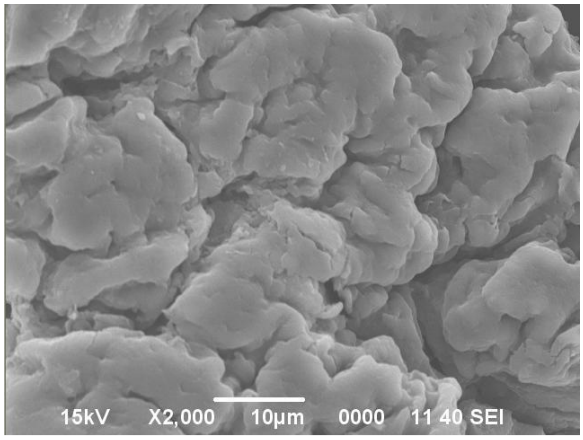

(a)

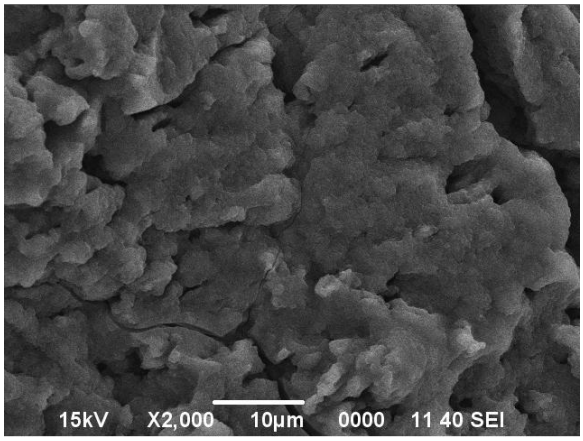

(b)

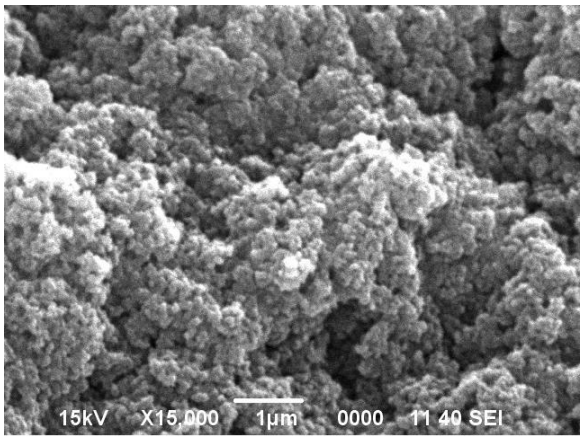

(c)

Fig. 4: Scanning electron micrographs of PPy.

UV-Vis analysis

UV-Vis spectra of the PPy correspond well with the conductivity of the polymer. UV-Vis measurements of PPy indicate three possible states of PPy existing all at the same time. These states are neutral PPy, polaron (radical cation) and bipolaron (dication). UV-Vis spectra of PPy solutions prepared in dimethylsufoxide (DMSO) are given in Fig. 5. All the three spectra show three characteristic bands. Band (a) around 256-270 nm is assigned to π—π* transition of the benzenoid ring in the PPy chains. Band (b) around 345-370 nm is attributed to polaron transition. Band (c) in the range of 630-650 nm is associated with bipolaron transition (n—π*) in the large π conjugated system of the polymer chain [28]. The last two bands are assigned to the doping level and introduction of polaron and bipolaron lattices, which represent the protonation stages of PPy chain. This behavior of the doped PPy causes an easier transition of electrons due to small energy gap and thus the conductivity of the polymer increases [29]. Considerably; a free carrier-tail broad band at about 700 nm is due to the extended coil of PPy chains showing a high degree of conjugation and thus high degree of doping and conductivity. Band (c) shows the spectrum of PPy 3 where the concentration of BPO was kept lower (1.2 x 10^{-3} mol) as compared to PPy 1 and PPy 2 (BPO = 1.2 x 10^{-2} mol). The change in the trend in PPy 3 spectrum as compared to other two samples is attributed to be due the frequent reduction of the BPO and hence the over oxidation of the polymer chain is reduced. The degree of oxidation and length of conjugated chain influence the doping level of the PPy that in turn affects the ratio of two absorption maxima [30].

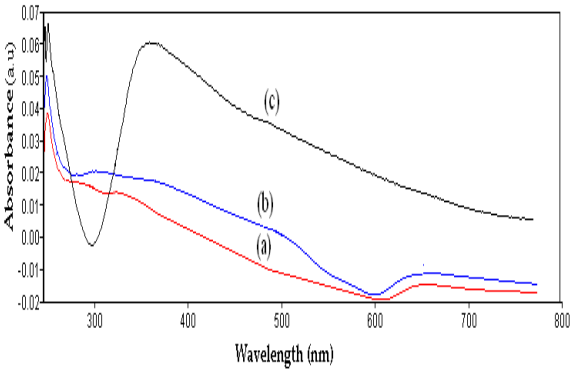

Fig. 5: UV-Vis spectra of PPy in DMSO [(a) PPy 1, (b) PPy 2 and (c) PPy 3.

Thermal Stability

The TGA characteristic of PPy was studied from room temperature to 650°C under N_2 (100cc/min) atmosphere. All the PPy samples were observed to exhibit three distinct weight losses as shown in Fig. 6. The first stage of weight loss (~5%) at about 80-100°C is associated with the evaporation of solvents, moisture and oligomers as well as unreacted monomers elimination. At further high temperature (170°C), a weight of about 35-40% occurs due to the loss of DBS^- component of the PPy. The drop in weight (~55-60%) observed at 200-400°C is due to the degradation of the PPy itself [**Error! Bookmark not defined.**]. PPy samples are thermally stable in the temperature range of 25-400°C and beyond this range; the decomposition route becomes very rapid. The residue weight of the PPy is about 40% in the nitrogen atmosphere, which is the carborized form (graphite structures) of the polymer. This indicates that PPy does not completely decompose in N_2 even at high temperature [**Error! Bookmark not defined.**, **Error! Bookmark not defined.**].

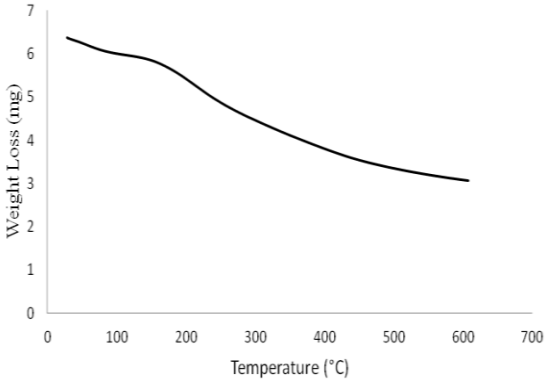

Fig. 6: TGA curve of PPy.

XRD analysis

XRD pattern indicates that the synthesized PPy powders exhibit a broad peak 2θ between 20°-30° which indicates some crystalline order in the bulk polymer powders. The two relatively broad peaks at around 21º and 23º illustrate the presence of crystalline domain in the amorphous PPy [31]. The appearance of these peaks in all the three PPy samples (Fig. 7) is caused due to the long DBSA alkyl chains that are non-uniformly spaced in PPy polymer main chains [32]. Also, the presence of DBSA causes conformational change to an ordered layer structure of PPy. A dramatic change in the crystallinity of PPy doped with DBSA depends on whether the polymer is cast from chloroform or *m*-cresol. PPy cast from chloroform are disordered as in the present investigation [33]. Sharp peaks at low angle (2θ = 10-20º) are assigned to the highly amphiphilic and aromatic sulphonate dopants (DBSA) and high angle 2θ is associated with the amorphous PPy chains. Sharps peaks show that the DBSA has successfully integrated in the polymer chain and gives a great degree of ordering to the PPy salts. The diffracting plane spacing (d), average chain separation (S) were calculated using the modified forms (2) and (3) of Bragg's equation and average crystallite size (t) by using Scherrer equation (4) [33] as given below:

$$d = \frac{n\lambda}{\sin\theta} \quad (2)$$

$$S = \frac{5\lambda}{8\sin\theta} \quad (3)$$

$$t = \frac{K\lambda}{\beta\cos\theta} \quad (4)$$

The comparative data obtained from these relations for the three PPy samples is summarized in Table-4. The results are in agreement with that reported in literature. These results confirmed the semicrystalline nature of PPy-DBSA salts.

Table-4: Parameters from XRD data.

Sample	Diffracting Plane Spacing'd' (Å)	Average Chain Separation 'S' (Å)	Crystallite Size 't' (nm)
Ppy 1	**3.79**	**4.74**	**16.22**
Ppy 2	**3.70**	**4.62**	**16.23**
Ppy 3	**3.83**	**4.78**	**16.21**

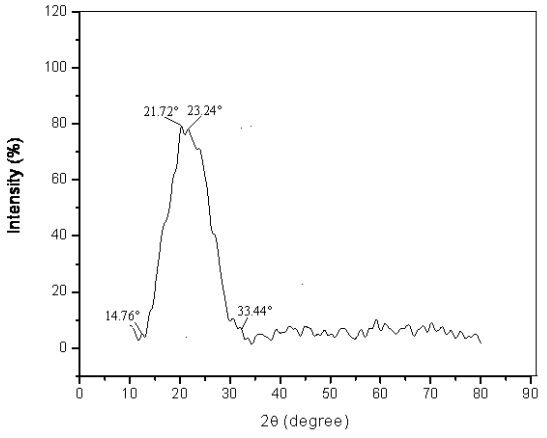

Fig. 7: XRD pattern of PPy.

Experimental

Pyrrole (Fluka Chemie) was distilled under vacuum. DBSA (Sigma Aldrich), Chlorofom (Sharlau), 2-butanol (Aldrich), Acetone (Scharlau), DMSO (Acros), THF (Sharlau), *m*-cresol (BDH Chemicals), and DMF (Acros) were used as received.

The emulsion polymerization was carried out in a 200 mL round bottom flask by taking 0.43 mol of chloroform in the flask. Then 0.012 mol of benzoyl peroxide was added to it under slow mechanical stirring. A white colour solution appeared within two minutes. Then 0.107 mol of 2-butanol, 3.9×10^{-3} mol of DBSA and 1.2×10^{-3} mol of pyrrole were added to the above solution. After adding 0.27 mol of distilled water to the above mixture, a milky white viscous emulsion was formed. The mixture turned brown in about thirty minutes and it was allowed to proceed for 24 hours upon vigorous stirring. At the end a black organic layer containing polypyrrole (PPy) was separated through a separating funnel. Then the PPy was washed three times with 20 mL of acetone and distilled water subsequently. PPy remained on the filter paper in the form of a thin layer which was allowed to dry for 12 hours at 70°C in an electric oven. As a result black powder of PPy was obtained. Similarly, other samples like PPy 2 and PPy 3 were synthesized with varying amounts of pyrrole (1.2×10^{-3} and 1.5×10^{-3} mol) and BPO (0.012 and 0.0012 mol), respectively.

FTIR analysis was carried out by using Shimadzu (IR Prestige-21) spectrometer (Japan). The FTIR spectrum of PPy was obtained by preparing a thin potassium bromide (KBr) pellet containing the sample. UV-Vis spectroscopy was done using Perkin Elmer UV-Visible spectrophotometer (USA). The XRD patterns of PPy were studied by JDX-3532 (JOEL Japan) X-ray diffractometer having a fixed radiation wavelength of λ=1.54A°. Thermal gravimetric analysis was carried out using Diamond TG/DTA (Perkin Elmer USA) analyzer. Scanning Electron Microscope Model JSM-5910 (JOEL Japan) was used for the analysis of surface morphology of PPy.

Conclusions

Soluble PPy was successfully synthesized via new inverse emulsion polymerization pathway. The formation of PPy was confirmed by FTIR. The data indicate incorporation of DBSA in the polymer backbone. TGA shows high thermal stability of the synthesized PPy up to ~ 450 °C. SEM and XRD analysis confirmed surface morphology and semi-crystalline nature of PPy respectively. The solubility of PPy in a variety of solvents and hence its processibility make it relatively good material for studying hitherto unavailable properties of the doped PPy.

References

1. G. G. Wallace, G. Spinks and P. R. Teasdale *Conductive Electroactive Polymer*, Technomic, New York, p. 60 (1997).
2. J. O. Iroh and C. Williams, *Synthetic Metals*, **8**, 8 (1999).
3. D. Kim, D. Lee and W. K. Paik, *Bulliten of Korean Chemical Society*, **27**, 710 (1996).
4. M. R. Gandhi, P. Murray, G. M. Spinks and G. G. Wallace, *Synthetic Metals*, **73**, 252 (1995).
5. J. H. Eung, S. J. Kwon and G. M. Alan, *Synthetic Metals*, **125**, 269 (2002).
6. J. Jang, *Advance Polymer Science*, **199**, 179 (2006).
7. S. J. Peighambardoust and B. Pourabbas, *Macromolecular Symposia*, **247**, 103 (2007).
8. A. Reung-u-Rai, A. P. J. Walaiporn, P. Q. Jai and S. Ouajai *Journal of Minerals Metals and Materials Society*, **18**, 29 (2008).
9. J. Stejskal, M. Omastova, S. Fedrova, J. Prokes and M. Trichova, *Polymer*, **44**, 1355 (2003).
10. Y. Shen and M. Wan, *Jounal of Polymer Chemistry*, **35**, 3692 (1997).
11. G. J. Lee, S. H. Lee, K. S. Ahn and K. H. Kim, *Journal of Applied Polymer Science*, **84**, 2587 (2002).
12. S. Bilal, S. Gul and A. A. Shah, *Synthetic Metals* **162**, 2259 (2012).
13. C. M. Li, C. Q. Sun, W. Chen and L. Pan, *Surface and Coatings Technology*, **198**, 475 (2005).
14. Q. Jianyong and L. Yongfang, *Polymer*, **38**, 3998 (1997).
15. M. A. Ghougule, S. G. Pawar, P. R. Godse, R. N. Mulik, S. Sen and V. B. Patil, *Soft NanoScience Letters*, **1**, 7 (2011).
16. K. T. Song, J. Y. Lee, H. D. Kim, D. Y. Kim, S. Y. Kim and C. Y. Kim, *Synthetic Metals*, **110**, 59 (2000).
17. M. Acik, C. Baristiran and G. Somez, *Journal of Material Science*, **41**, 4680 (2006).
18. M. Omastova, M. Trehova, J. Poionteck, J. Prokes and J. Stejskal, *Synthetic Metals*, **143**, 167 (2004).
19. M. K. Song, Y. T. Kim, B. S. Kim, J. Kim, K. Char and H. W. Rhee, *Synthetic Metals*, **141**, 317 (2004).
20. K. R. L. Castagno, V. Dalmoro and D. S. Azambuja, *Materials Chemistry and Physics*, **130**, 724 (2011).
21. F. Fusalba and D. Belanger, *Journal of Physical Chemistry*, **103**, 9050 (1999).

22. M. R. Karim, C. J. Lee, A. M. S. Chowdury, N. Nahar and M. S. Lee, *Materials Letters*, **61**, 1691 (2007).
23. J. Lei and C. R. Martin, *Synthetic Metals*, **48**, 334 (1992).
24. P. Mavinakuli, S. Wei, Q. Wang, A. B. Karki, S. Dhage, Z. Wang, D. P. Young and Z. Guo, *Journal of Physical Chemistry*, **114**, 3878 (2010).
25. H. W. Eisazadeh, *Journal of Chemistry*, **2**, 70 (2007).
26. J. Jooa, J. K. Lee, J. S. Baecka, K. H. Kimb, E. J. Oh and J. Epsteind, *Synthetic Metals*, **117**, 49 (2001).
27. P Javamurugan, V. Ponnuswany, S. Deivanayaki, P. Maddeswara and J. Chandrasekaran, *Opto Electronics and Advanced Materials Rapid Communications*, **4**, 554 (2010).
28. B. R. Saunders, K. S. Murray and J. Robert, *Chemistry of Materials*, **6**, 703 (1994).
29. Y. Shen and M. Wan, *Synthetic Metals*, **96**, 130 (1998).
30. L. I. BaoSong, Q. I. HongXu, Z. W. Tao, Z. YaLing, Z. Xiang, L. I. ShuXi and W. Yan, *Science China Technological Sciences*, **54**, 1700 (2011).
31. W. Prissanaroo, N. Bark, P. J. Pigram, J. Liesegang and T. J. Cardwell, *Surface and Interface Analaysis*, **33**, 668 (2002).
32. C. Basavaraja, W. J. Kim, D. G. Kim and D. S. Huh, *Polymer Composites*, **33**, 393 (2012).
33. S. M. Ebrahim, A. Gad and A. Morsy, *Synthetic Metals*, **160**, 2661 (2010).